The Photophysics of Free-Base Hemiporphyrazine: A Theoretical Study

Verdiana Persico, Maurizio Carotenuto, and Andrea Peluso*

Dipartimento di Chimica, Università di Salerno, I-84081 Baronissi, Salerno, Italy

Received: December 6, 2003; In Final Form: February 25, 2004

The photophysics of free-base hemiporphyrazine has been studied by theoretical computations based on time dependent density functional theory and multiconfigurational complete active space methods. The results confirm that the dual emission spectrum of hemiporphyrazine is due to the formation at the excited state of different tautomers, but the emission at longer wavelength, originally attributed to a vibronically induced radiative decay from the tautomer with both central hydrogens linked to pyridine rings, is now ascribed to a dipole allowed transition, occuring either from that tautomer or from the tautomer with the two hydrogens linked to one pyridine and one isoindole ring.

Introduction

Free-base hemiporphyrazine (HpH_2), the phthalocyanine analogue where two opposite faced isoindoles are replaced by two pyridine rings,[1,2] exhibits a peculiar photophysical behavior, significantly different from that of other macrocycles of porphyrin and phthalocyanine families. HpH_2 absorbs at much shorter wavelengths than porphyrins, 350 nm, and shows a dual emission, peaked at 420 and 670 nm, which has been attributed to the formation at the excited state of different tautomers.[3,4] In fact, because the four inner nitrogens of the macrocycle are not chemically equivalent, three tautomeric forms of HpH_2, differing for the positions of the two central hydrogens, can formally be written; the inner hydrogens both can be linked to the isoindoles or to the pyridine rings, tautomers A and B respectively, or to one isoindole and one pyridine ring, tautomer C, see Figure 1.

In the ground state **A** is expected to be the prevalent form, because it exhibits 2^4 resonance structures, whereas only half of them can be drawn for both **B** and **C**. Further support to this conjecture is provided by the NMR and the infrared spectra of germanium and tin Hp complexes.[5,6] Furthermore, the X-ray structures of Hp metal derivatives show a clear-cut alternation of shorter and longer bond distances between all the meso nitrogens and the pyridine and isoindole α carbons.[7,8] That is peculiar of **A** (see the optimized structures below), for which the delocalization pathway of the π electrons is not extended to the whole macrocycle, but mainly concerns the pyridine and the isoindole benzene rings. On the contrary, **B** exhibits two resonance structures involving $4n$ π electrons ($n = 5$) and spanning the whole macrocycle, see Figure 1. Thus the electronic structure of **B** appears to be more similar to those of related macrocycles such as porphyrins and phthalocyanines, and therefore it should absorb at longer wavelengths than **A** and **C**.

On the basis of the above argumentations and with the aid of semiempirical MNDO/CI computations, the absorption at 350 nm and the emission at 420 nm have been assigned to **A**, whereas the emission peak at 670 nm has been assigned to **B**, which is formed, upon **A** excitation, via a double hydrogen atom transfer. However, the longer wavelength transition predicted by MNDO/CI computations for B is forbidden in D_{2h} symmetry, so that vibronic intensity borrowing must be invoked for that transition (MNDO/CI computations yield a very low electric dipole transition moment, because of slight distortions of the minimum energy geometry from the D_{2h} symmetry). Tautomer **C** can also be formed at the excited state; indeed, a very weak band at 550 nm has been tentatively assigned to **C** emission.[4] **C** could be a short living intermediate along the reaction path leading from **A** to **B**, according to a stepwise mechanism, but it could also be a photochemical product formed in competition with **B**.

The photophysics of HpH_2 is therefore very interesting, with several radiationless decay paths involving three different tautomeric forms in competition between them. In this paper, with the purpose of providing a better assignment of the spectral signals and of guiding further experimental work aimed to understand the dynamics of excited-state hydrogen atom transfer, we report a theoretical study of the lowest excited states of the three tautomers of HpH_2 based on ab initio multiconfigurational self-consistent field (MCSCF) and time dependent density functional theory (TDDFT) computations.

Computational Details

The minimum energy structures of the three tautomers have been computed by full geometry optimization at the DFT level of computations using the split valence 6-31g basis set. All the optimization runs start from structures with D_{2h} symmetry for tautomers **A** and **B** and C_s symmetry for tautomer **C**; all the computed minimum energy structures retain the above symmetries. The hybrid B3LYP exchange correlation potential (Becke's three parameter hybrid function[9] with the nonlocal correlations of Lee−Yang−Parr[10]) have been employed in all DFT computations. Ground-state energies have been computed at the DFT level, using the 6-311g(d,p) basis set, and compared with those previously obtained by RHF/MP2 calculations.[4] The G98 package[11] was employed for ab initio and DFT computations.

The vertical transition energies for the lowest excited singlet states of the three tautomers have been computed by second-order perturbation theory with a multiconfigurational reference state, the so-called CASPT2 method,[12−14] using the MOLPRO package.[14,15] The RHF/6-31g optimized geometries and the standard 6-31g(d) basis set have been adopted in the CASPT2

* Corresponding author. E-mail apeluso@chem.unisa.it

10.1021/jp037736d CCC: $27.50
Published on Web 04/10/2004

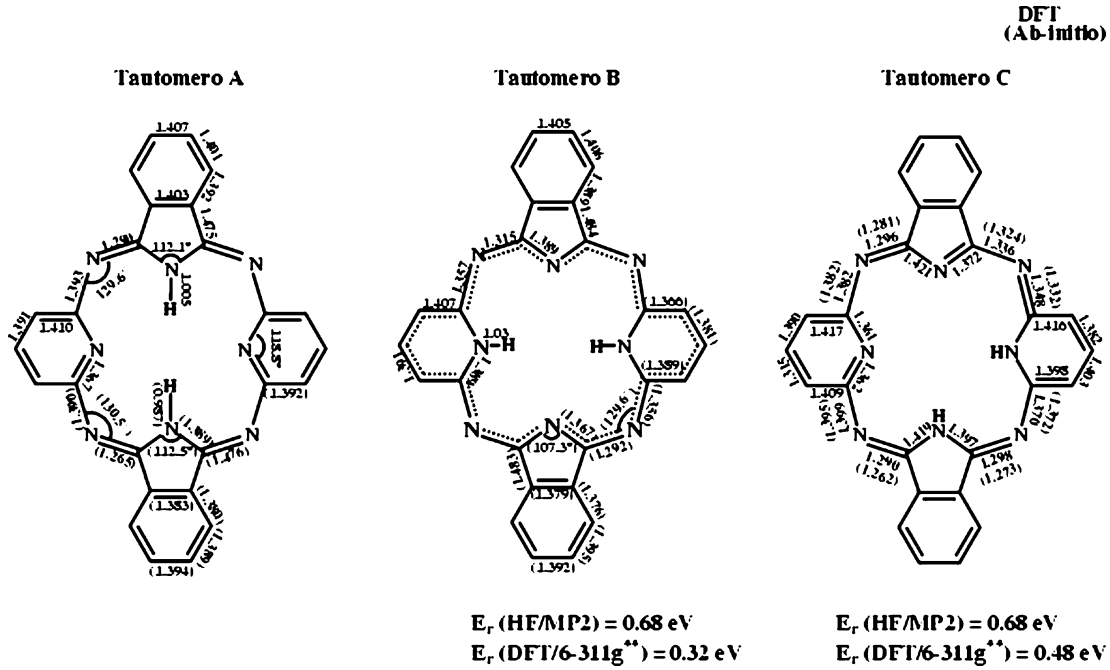

Figure 1. Selected geometrical parameters and relative energies of the ground states of the three tautomers of HpH_2 obtained by DFT and ab initio (in parentheses) computations. Bond distances are in Å, angles in degrees, relative energies in eV.

computations, use of larger basis sets being ruled out by the size of the molecules. Since for large size molecules such as hemiporphyrazine the convergence of the CASPT2 results with respect to the size of the adopted basis set and active space cannot be properly addressed, the time-dependent DFT method[16] with 6-31g(d,p) and 6-311g(d,p) basis sets was also employed for comparison, using the minimum energy geometries obtained by DFT/B3LYP/6-31g optimizations. The active spaces used in CASPT2 computations have been chosen in such a way that the first-order corrections to the wave functions yielded by the perturbative treatment are of the same order of magnitude for both the ground and the excited states. A level shift[17] of 0.4 au has been used throughout computations.

Results

Ground States. The ground-state geometries and the relative energies of the three tautomers obtained at different level of computations are reported in Figure 1.

Both ab initio and DFT computations indicate that **A** is the most stable form of HpH_2 in the ground state, cf. Figure 1. The computed energy differences are sufficiently high for ruling out the existence of **B** and **C** at room temperature.

Selected geometrical parameters are reported in Figure 1. The bond distances between the meso nitrogens and the α carbons of the pyridine and isoindole rings are suitable parameters for judging the π delocalization in the three tautomers. Both ab initio and DFT computations predict a clear-cut alternation of shorter and longer $C-N_{meso}$ bond distances in **A**, which compare very well with those obtained from X-ray diffraction data of the Ge Hp metal complex (1.274 and 1.380 Å for the bond distances between the meso nitrogens and the isoindole and pyridine carbons, respectively). A very similar pattern is found for **C**, but for the region between the unprotonated isoindole and the protonated pyridine rings, where both DFT and ab initio predict very similar $C-N_{meso}$ bond distances. That could be due to a significant weight of a charge separated resonance structure, with the positive and negative charges localized on the protonated pyridine and the unprotonated isoindole rings. Mulliken's

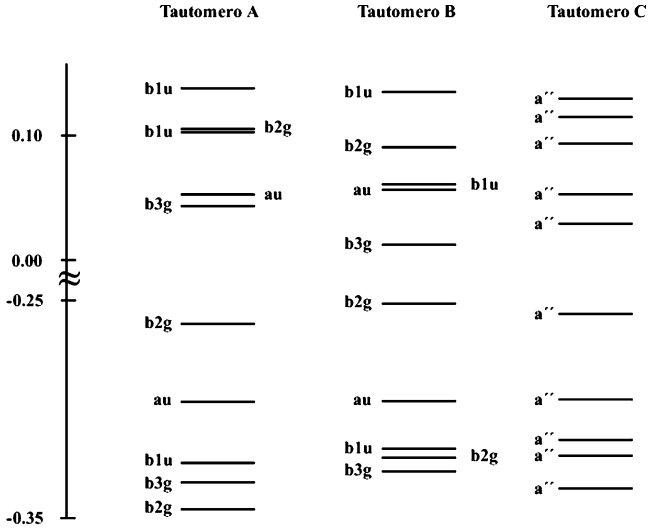

Figure 2. Molecular orbitals of the ground electronic states of the three tautomers as obtained by RHF/6-31g computations.

population analysis confirms that conjecture; the protonated pyridine ring in **C** carries a positive charge, 0.71 (0.99) a.u. at DFT (RHF) level of computation, which is significantly higher than its counterpart in **A**, 0.31 (0.49). Because of that, **C** exhibits a slightly longer delocalization pattern of the π electrons than **A**, which includes the protonated pyridine ring and the unprotonated isoindole ring. For **B**, the bond distances between the meso nitrogen and the α carbons of the two rings are much more similar each other, since two resonant structures spanning the whole macrocycle can be written for this tautomer, as shown in Figure 1.

Excited States. The molecular orbital (MO) occupation scheme obtained from HF computations is shown in Figure 2. The HOMO and the LUMO of **A** and **B** are both of gerade symmetry (b_{2g} and b_{3g}, respectively), so that the HOMO→LUMO transition gives rise to a "dark" B_{1g} state. The LUMO+1 (a_u) is also very low in energy so that a "light" B_{2u} state, arising from the promotion of an electron from the HOMO to the LUMO+1 could be among the lowest excited states of both **A**

TABLE 1: Transition Energies (ΔE eV) and Electric Dipole Transition Moments (d a.u.) for the Lowest Energy Excited Singlets of A

	DFT				CASPT2	
	ΔE(6-31g(d,p))	$\vec{\mathbf{d}}$	ΔE(6-311g(d,p))	$\vec{\mathbf{d}}$	ΔE	$\vec{\mathbf{d}}$
B_{1g}	2.27	0.0	2.49	0.0	2.22	0.0
B_{2u}	3.12	2.17	3.31	2.23	3.43	3.66
B_{2g}	3.40	0.0	3.50	0.0	2.88	0.0
B_{3u}	3.48	2.17	3.68	2.14	3.71	3.04
B_{1u}	3.65	0.18	3.73	0.15	3.24	0.46

and **B**. As concerns the other electronic states of **A** and **B** with nonzero electric dipole transition moments with the ground state, states B_{1u} and B_{3u}, the latter can be obtained by the HOMO-1→ LUMO transition, being also expected to fall at comparatively low energy, whereas the former is obtained by promoting an electron from the lower lying b_{2u} and b_{1g} MOs to the LUMO and LUMO+1, respectively, so that it should fall at higher energy. For **C**, both the highest occupied MO and the lowest unoccupied ones are of a″ type, see Figure 2, so that the lowest excited singlet states are expected to be A′ states, with electric dipole transition moments polarized in the molecular plane.

In the CASPT2 treatment we have focused attention mainly on those electronic states which characterize the absorption and emission spectra of HpH_2; as concerns other states, which could be important in discussing radiationless transition and excited-state tautomerization processes, we have limited CASPT2 computations to those which, from the MO analysis and TDDFT results, are expected to be lower in energy.

The energies of the lowest lying excited singlets of **A** together with the electric dipole transition moments are reported in Table 1. In the CASPT2 computations we have used two active spaces, one involving 16 electrons and 13 MOs, the other involving 12 electrons and 12 MOs, hereafter denoted as (16,13) and (12,-12). The (16,13) active space includes three b_{1u},b_{2g} and a_u MOs, two occupied and one empty, and four b_{3g} MOs, two occupied and two unoccupied. That space is well suited for electronic states of B_{1g}, B_{2u}, B_{3u}, and A_g symmetry. For the B_{1u} state, the (12,12) active space includes the highest occupied and lowest unoccupied b_{2u}, b_{3u}, b_{2g}, and b_{3g} MOs, one occupied MO of a_g and b_{1g} symmetry and one empty MO of b_{1u} and a_u symmetry. The same active space was also used for the B_{2g} state, with the only difference of replacing the occupied b_{3g} MO with the a_u one and the empty b_{3u} with the a_g one.

As expected from the above analysis, the lowest excited singlets of **A** at both levels of calculation is the B_{1g} state. The transition energies predicted by TDDFT and CASPT2(16,13) methods are 2.49 and 2.22 eV, respectively. Both methods predict that only the HOMO→LUMO transition significantly contribute (> 96%) to that state.

The next singlet states at the CASPT2 level are the B_{2g} and the B_{1u}, with transition energy 2.88 and 3.24 eV. The main contributions to the wave function of the former state is given by one electron transition from the highest occupied b_{1g} MO to the LUMO (50%) and from the highest occupied b_{2u} MO to the LUMO+1 (30%). The wave function of the first excited B_{1u} state is characterized by two one-electron transitions, from the highest b_{3u} MO to the LUMO (50%) and from the highest b_{1g} to the LUMO+1 (50%). For both states, TDDFT predict higher transition energies; the lowest B_{1u} state is predicted to fall at 3.65 eV, at higher energy than both the B_{2u} and B_{3u} states, whereas the transition energy of the B_{2g} state is predicted to be 3.40 eV, so that it falls midway in energy between the B_{2u} and B_{3u} states. Although the energy ordering predicted by TDDFT is in line with that expected from the MO analysis, the results of CASPT2 computations better match the experimental data. In fact the absorption spectrum of HpH_2 exhibits a pronounced shoulder at longer wavelengths, which could be assigned to the weak A_g→B_{1u} transition. Both CAS and TDDFT computations yield for the B_{1u} state a weak transition moment, polarized along the axis perpendicular to the molecular plane. As concerns the "dark" B_{2g} there is experimental evidence from two-photon absorption spectroscopy that a gerade state must fall in the region between 2.9 and 3.2 eV,[18] thus in line with the transition energy obtained by CASPT2 computation for the first B_{2g} singlet.

TABLE 2: Transition Energies (ΔE eV) and Electric Dipole Transition Moments (d a.u.) for the Lowest Energy Excited Singlets of B

	DFT				CASPT2	
	ΔE(6-31g(d,p))	$\vec{\mathrm{d}}$	ΔE(6-311g(d,p))	$\vec{\mathrm{d}}$	ΔE	$\vec{\mathbf{d}}$
B_{1g}	1.56	0.0	1.57	0.0	0.70	0.0
B_{2u}	2.78	1.37	2.78	1.48	2.41	3.00
B_{2u}	2.98	0.0	2.98	0.0	2.83	1.76
B_{2g}	2.97	1.43	3.00	1.39	2.24	0.0
B_{1g}	3.03	0.0	3.04	2.34	2.92	0.0
B_{3u}	3.09	0.08	3.07	0.08	3.02	0.50

The two most important states for assigning spectroscopic signals are the B_{2u} and the B_{3u} states. For those states there is very good agreement between TDDFT and CASPT2, the computed transition energies are in fact 3.31 and 3.68 eV (TDDFT) and 3.43 and 3.71 (CASPT2) for the B_{2u} and the B_{3u} states, respectively. Both methods yield that the B_{2u} state is mainly given by the promotion of an electron from the HOMO to the LUMO+1 (76% in TDDFT, 87% in CASPT2), with the remaining contribution given by the promotion of an electron from the HOMO-2 (b_{1u}) to the LUMO (b_{3g}). The B_{3u} state is essentially given by the HOMO-1→LUMO transition. Thus, at least as concerns the last two states, the most important for the absorption spectrum of HpH_2, a four-level model similar to Gouterman's one for porphyrin[19] can also be applied to HpH_2 in its most stable form **A**.

The electric dipole transition moments ($\vec{\mathbf{d}}$) of the two lowest states of ungerade symmetry have different polarization (D_{2h} symmetry): for the B_{2u} state the electric transition moment is directed along the axis passing through the two pyridine nitrogens, whereas for the B_{3u} state it is directed along the perpendicular axis, passing through the two central protons.

The energies of the lowest lying excited singlets and the electric dipole transition moments of **B** are reported in Table 2. In the CASPT2 computations we have used the same active spaces used for **A**. Inspection of the transition energies reported in Table 2 shows that the excited singlets of **B** are all significantly lower in energy than those of **A**, as expected from the longer delocalization pathway which characterizes the π electrons of **B** with respect to that of **A**. Similarly to **A**, the lowest excited singlet of **B** is the "dark" B_{1g} state, arising from the HOMO→LUMO transition. That state is predicted by TDDFT at 1.56 eV above the ground state, whereas CASPT2 yields a transition energy of only 0.7 eV. This is the largest discrepancy between TDDFT and CASPT2 results found in this paper. Since the B_{1g} is a dark state, we have not further investigated this case.

As concerns states which can give rise to allowed transitions, computations yield two B_{2u} states falling at 2.78 and 2.98 eV, according to TDDFT, and at 2.41 and 2.83 eV, according to CASPT2. Two transitions contribute to the wave functions of both states, the HOMO→LUMO+1 (50% in $1B_{2u}$, 25% in $2B_{2u}$) and the HOMO-2→LUMO (30% for $1B_{2u}$, 50% for $2B_{2u}$). For

TABLE 3: Transition Energies (ΔE eV) and Electric Dipole Transition Moments (d a.u.) for the Lowest Energy Excited Singlets of C

	DFT				CASPT2[a]	
	ΔE(6-31g(d,p))	$\vec{d}$	ΔE(6-311g(d,p))	$\vec{d}$	ΔE	$\vec{d}$
A′	1.85	0.27	1.85	0.26	1.98	0.48
A′	2.88	1.66	2.88	1.74	3.34	3.63
A″	2.88	0.02	2.90	0.02	3.46	
A′	3.04	1.01	3.03	1.06		

[a] No level shift has been used in CASPT2 computations.

both states the transition moments are polarized along the axis passing through the protonated pyridine nitrogens. Slightly above the two B_{2u} states, there is the first B_{3u} singlet, arising by the promotion of an electron from the HOMO-1 to the LUMO. Both TDDFT and CASPT2 predict that this state is ca.3.0 eV above the ground state, with the electric dipole transition moment polarized along the axis lying in the molecular plane and perpendicular to the polarization axis of the B_{2u} states.

The energies of the lowest lying excited singlets and the electric dipole transition moments of **C** are reported in Table 3. The fact that **C** possesses only a plane of symmetry significantly limits the size of the active space to be used in computations. The largest active space we were able to use for A′ states includes eight electrons and ten MOs, all of a″ symmetry, whereas for the first A″ state, the (8,10) active space includes one occupied and one unoccupied a′ MO.

The lowest two excited states of **C**, both of A′ symmmetry, are predicted by TDDFT computations to fall at 1.85 and 2.88 eV above the ground state, in reasonable agreement with CASPT2 computations, yielding transition energies of 1.98 and 3.34. The lowest excited singlet mainly corresponds to the pure HOMO→LUMO transition (95%), whereas several electronic transitions contribute to the wave function of the 2 A′ state, i.e., the HOMO→LUMO+1 (70%), the HOMO-2→LUMO (10%), and the HOMO-4→LUMO (10%). Both methods predict that the lowest excited singlet has a weak electric dipole transition moment, lying in the molecular plane and oriented midway between the protonated isoindole and the unprotonated pyridine rings, whereas the second one exhibits a strong transition moment oriented along the axis passing through the two pyridine nitrogens. The other low lying excited singlets of **C** yielded by TDDFT are a A″ state, mainly given by the HOMO-3→LUMO transition, and a pair of light A′ states, falling at 3.0 and 3.1 eV and arising by transitions from the inner occupied a″ MOs to the LUMO and LUMO+1.

The Absorption and Emission Spectra. The absorption spectrum of HpH_2 is characterized by a strong transition peaked at 350 nm (3.5 eV) with a shoulder around 420 nm (3.0 eV), followed by a strong increase in absorption at wavelengths shorter than 330; no signal is detected at wavelengths longer than 450−500 nm.[20,21]

The computed relative energies rule out the possibility that at the ground state both **B** and **C** are present, so that the absorption spectrum has to be entirely assigned to transitions of **A**. Furthermore, both TDDFT and CASPT2 yield for **B** and for **C** allowed transitions in the region of longer wavelengths, 500−700 nm, which is another evidence that **B** and **C** can be formed only upon excitation of the most stable form, since no signal is observed in that region.

The results of all the computations referring to the absorption spectrum of HpH_2 are summarized in Figure 3a. According to the computed transition energies, the intense peak at 350 nm can be assigned to the $^1A_g \rightarrow {}^1B_{2u}$ transition and the strong

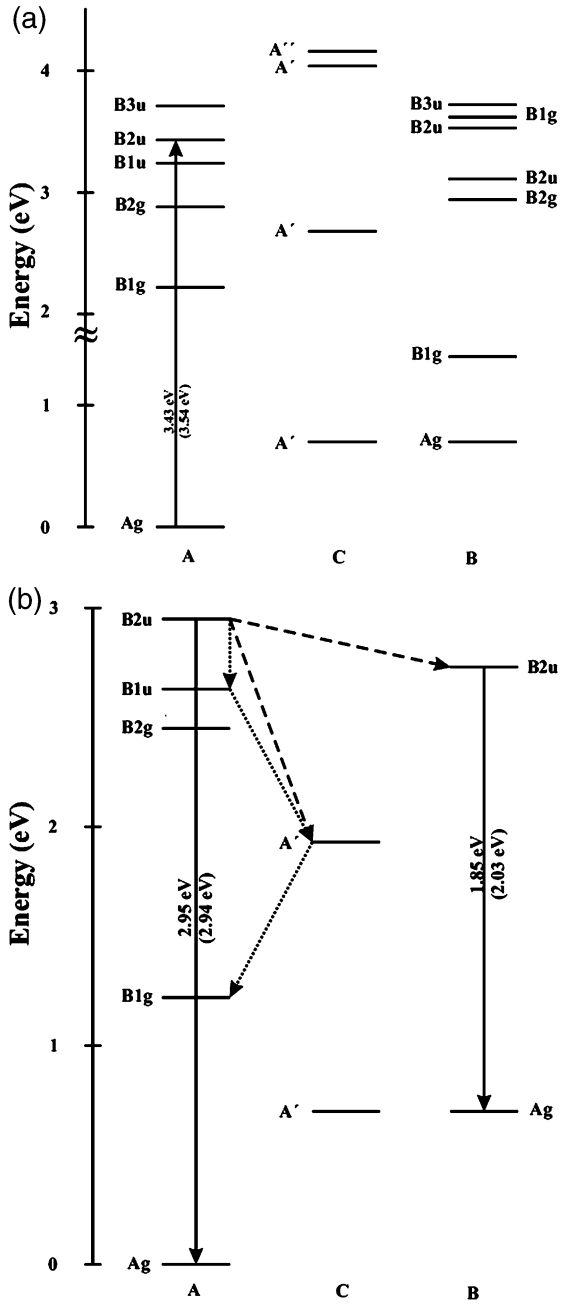

Figure 3. Sketch of the possible radiative and nonradiative decay paths of free-base hemiporphyrazine according to the computed CASPT2 energies of the lowest excited singlets of the three tautomers (experimental values in parentheses): (a) ground-state optimized geometries; (b) excited-state optimized geometries.

increase in the absortion starting from 330 nm to the $^1A_g \rightarrow {}^1B_{3u}$ one. Both transitions have large electric dipole transition moments, polarized along perpendicular axes lying in the molecular plane. Furthermore, CASPT2 predicts a weak $^1A_g \rightarrow {}^1B_{1u}$ transition at 3.24 eV, to which the shoulder observed at 420 nm can be assigned.

The emission spectrum of HpH_2 is characterized by two well-separated weak bands, a broad one peaked at 420 nm and a much narrower one peaked at 675 nm. The energy ordering of the excited states plays a crucial role in the assignment of emission spectra, because of the involvement of radiationless decays. Thus it is important to keep in mind that the computed transition energies are certainly affected by errors, both for the smallness of the adopted basis set and for the large level shift

used in the perturbative treatment, and therefore they have to be used with great caution.

There are a few pieces of evidence which suggest that the broad emission at 420 nm has to be assigned to **A**. First, the emission band appears as the mirror image of the absorption spectrum, with its maximum located almost at the same wavelength of the shoulder in the absorption peak. Second, the ground-state energies computed at HF/MP2 level rule out the possibility that it is originated by a radiative decay from any of the excited states of both **B** and **C**. The ground state of the last two tautomers are in fact about 0.7 eV higher in energy than the **A** one, so that the electronic state responsible for that emission should be located about 3.6−3.7 eV above the ground state of **A**, but the emission at 420 nm (2.95 eV) is observed also by exciting the sample at 380 nm (3.26 eV).[4] The above possibility is also hardly compatible with DFT computations, which predict that the ground state of **B** is 0.32 eV above that of **A**. Thus, the computed transition energies summarized in Figure 3a suggest that the band peaked at 420 nm could be assigned either to the $^1B_{1u} \rightarrow {}^1A_g$ or to the strong $^1B_{2u} \rightarrow {}^1A_g$ radiative transitions of **A**, or, because of its broadness, to both.

As concerns the emission at longer wavelengths, there are several possible assignments: a good candidate would be the symmetry allowed transition $2A' \rightarrow 1A'$ of **C**. That transition is not only predicted in the right energy range, at 2.0 eV, but the 2 A′ state of **C** is also the lowest excited state of **C**, thus satisfying Kasha's rule. Moreover, the hypothesis that this transition is vibronically induced, necessary in the previous assignment of that band to emission of **B**,[4] would be no longer needed. There are, however, two other transitions to which the longer wavelength emission could be assigned: the electric dipole forbidden $^1B_{1g} \rightarrow {}^1A_g$ of **A** and the allowed $^1B_{2u} \rightarrow {}^1A_g$ of **B**.

The transition energies reported in Figure 3a refer to vertical transition from the optimized geometry of the ground states and as such they can give only reasonable indications on the emission spectrum of HpH_2. To better discriminate among the above hypotheses, the low lying excited states of HpH_2 have been optimized at the CASSCF level and the optimized geometries have then been used to evaluate vertical emission energies at the CASPT2 level. D_{2h} symmetry constraints have been imposed in the optimization of the lowest excited states of **A** and **B**, and C_s symmetry constraints for those of **C**; that choice has been dictated by the size of the system under study, but it is worth mentioning that there is no experimental evidence supporting it.

To better clarify also the origin of the shorter wavelength emission, the lowest four excited states of **A** have been optimized, whereas for **B** and **C** it is sufficient to optimize only the lowest "light" excited state. The most interesting geometrical parameters of the optimized geometries of these excited states are reported in Table 4, together with the vertical transition energies and the energy differences with respect to the optimized ground-state energies, which, neglecting changes in the zero point energies, give transition energies between ground vibrational states.

The energy orderings of the optimized electronic states are summarized in Figure 3b, together with the possible radiationless decay paths. As concerns the broad band peaked at 420 nm, the vertical transition from the B_{2u} singlet of **A** is predicted at 2.95 eV, in good agreement with the experimental result. Also the B_{1u} state can contribute to the broad emission, since its radiative emission is predicted in the range 2.63−3.10 eV (470−400 nm). It is remarkable that this radiative emission is not quenched by the "dark" B_{2g} state, located just below the B_{1u} state. The possibility that the energy of this state is underestimated by CASPT2 computations, as suggested by TDDFT computations, cf. Table 1, seems to be ruled out by preliminary two-photon-induced fluorescence, which confirms the energy ordering predicted by CASPT2 computations.[18] Thus, the fact that a broad emission peaked at 420 nm is indeed observed is due certainly to the strength of the $B_{2u} \rightarrow A_g$ transition and possibly to the fact that the B_{1u} and the B_{2g} states are nearly degenerate.

TABLE 4: Optimized Bond Distances (Å) between the meso Nitrogens and the α Isoindole and Pyridine Rings (CASSCF computations) and Transition Energies (eV) (CASPT2, level shift = 0.4) for Some Lowest Lying Excited States of HpH_2

				transition energy	
tautomer	state	N−C_{iso}	N−C_{pyr}	vertical	0−0
A	B_{1g}	1.31	1.33	1.23	1.62
A	B_{2g}	1.28	1.38	2.45	2.69
A	B_{1u}	1.28	1.39	2.63	3.10
A	B_{2u}	1.29	1.35	2.95	3.05
B	B_{2u}	1.32	1.32	2.03	2.24
C	A′	1.31[a]	1.33[a]	1.23	1.72

[a] Average value.

As concerns the emission at longer wavelength (675 nm), its assignment to the $B_{2u} \rightarrow A_g$ transition of **B** appears to be the most plausible one, both for the computed vertical transition energy (2.03 eV) and for the predicted strength of that transition. Both the B_{1g} state of **A** and the 2A′ state of **C** are significantly stabilized by geometry optimization, the vertical emission energy being predicted at about 1.2 eV for both states. However, the possibility that the longer wavelength emission is originated by the radiative decay between the ground vibrational states of the lowest two A′ states of **C** is left open by computations, since the 0−0 transitions is significantly higher in energy (1.73 eV) than the vertical transition. The 0−0 $B_{1g} \rightarrow A_g$ transition of **A** (1.62 eV) is forbidden, but, since the B_{1g} of **A** is predicted to be the lowest energy excited state among all three tautomers of HpH_2, the possibility that efficient radiationless decays lead to a large population of that state, followed by a weak, vibronically induced, radiative decay, cannot be discarded. Thus, although computational techniques have proved beyond doubt to be a valuable interpretative tool, further experimental studies, in particular time-resolved spectroscopy and two-photon-induced fluorescence, are necessary for a conclusive assignment of that signal; work is in progress along this line.

Acknowledgment. We are indebted to one of the reviewers for very helpful suggestions. The financial support of the University of Salerno is gratefully acknowledged. We also thank the CIMCF, Dipartimento di Chimica, Università Federico II, Naples (Italy), for providing computational facilities.

References and Notes

(1) Fernández-Lázaro, F.; Torres, T.; Hauschel, B.; Hanack, M. *Chem. Rev.* **1998**, *98*, 563.
(2) Elvidge, J. A.; Linstead, R. P. *J. Chem. Soc.* **1952**, 5008.
(3) Peluso, A.; Garzillo, C.; Del Re, G. *Chem. Phys.* **1996**, *204*, 347.
(4) Altucci, C.; Borrelli, R.; de Lisio, C.; De Riccardis, F.; Persico, V.; Porzio, A.; Peluso, A. *Chem. Phys. Lett.* **2002**, *354*, 160.
(5) Sutton, L. E.; Kenney, M. E. *Inorg. Chem.* **1967**, *6*, 1869.
(6) Esposito, J. N.; Sutton, L. E.; Kenney, M. E. *Inorg. Chem.* **1967**, *6*, 1116.
(7) Hecht, H.; Luger, P. *Acta Crystallogr. B* **1974**, *30*, 2843.
(8) Speakman, J. C. *Acta Crystallogr.* **1953**, *6*, 784.
(9) Becke, A. D. *Chem. Phys. J.* **1993**, *98*, 5648.
(10) Lee, C.; Yang, W.; Parr, R. G. *Phys. Rev. B* **1988**, *37*, 785.

(11) Gaussian 98, Revision A.7, Frisch, M. J.; Trucks, G. W.; Schlegel, H. B.; Scuseria, G. E.; Robb, M. A.; Cheeseman, J. R.; Zakrzewski, V. G.; Montgomery, J. A., Jr.; Stratmann, R. E.; Burant, J. C.; Dapprich, S.; Millam, J. M.; Daniels, A. D.; Kudin, K. N.; Strain, M. C.; Farkas, O.; Tomasi, J.; Barone, V.; Cossi, M.; Cammi, R.; Mennucci, B.; Pomelli, C.; Adamo, C.; Clifford, S.; Ochterski, J.; Petersson, G. A.; Ayala, P. Y.; Cui, Q.; Morokuma, K.; Malick, D. K.; Rabuck, A. D.; Raghavachari, K.; Foresman, J. B.; Cioslowski, J.; Ortiz, J. V.; Baboul, A. G.; Stefanov, B. B.; Liu, G.; Liashenko, A.; Piskorz, P.; Komaromi, I.; Gomperts, R.; Martin, R. L.; Fox, D. J.; Keith, T.; Al-Laham, M. A.; Peng, C. Y.; Nanayakkara, A.; Gonzalez, C.; Challacombe, M.; Gill, P. M. W.; Johnson, B.; Chen, W.; Wong, M. W.; Andres, J. L.; Gonzalez, C.; Head-Gordon, M.; Replogle, E. S.; Pople, J. A. Gaussian, Inc., Pittsburgh, PA, 1998.

(12) Roos, B. O.; Andersson, K.; Fülscher, M. P.; Malmqvist, P. Å.; Serrano-Andres, L. *Adv. Chem. Phys.* **1996**, *XCIII*, 219.

(13) Andersson, K.; Malmqvist, P. A.; Roos, B. O. *J. Chem. Phys.* **1992**, *96*, 1218.

(14) Celani, P.; Werner, H. J. *J. Chem. Phys.* **2000**, *112*, 5546.

(15) Werner, H. J.; Knowles, P. J. MOLPRO, version 2002−3.

(16) Runge, E.; Gross, E. K. U. *Phys. Rev. Lett.* **1984**, *52*, 997.

(17) Roos, B. O.; Andersson, K. *Chem. Phys. Lett.* **1995**, *245*, 215.

(18) de Lisio, C., private communication.

(19) Gouterman, M. *The Porphyrins*, Academic Press Inc.: New York, 1978; Vol 3, p 1.

(20) Elvidge, J. A.; Linstead, R. P. *J. Chem. Soc.* **1952** 5008.

(21) Bossa, M.; Grella, I.; Nota, P.; Cervone, E. *J. Mol. Struct. (THEOCHEM)* **1990**, *210*, 267.